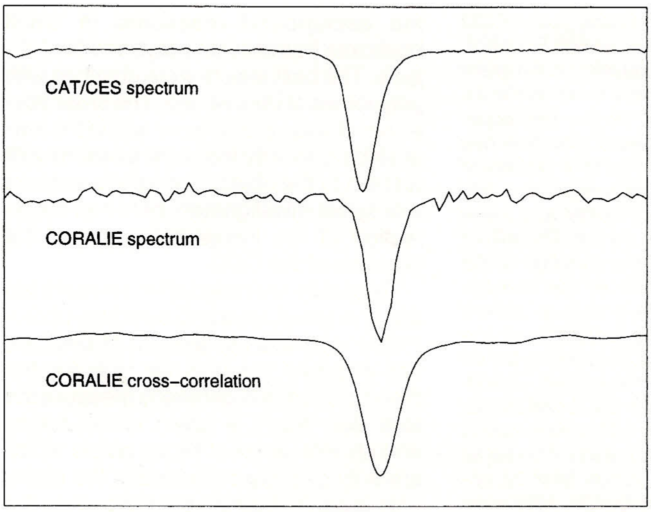

Figure 3: A Si II 4130Å line profile obtained with the CAT/CES is compared with one obtained with CORALIE and a cross-correlation profile derived from the CORALIE spectrum. Integration times were 25 minutes for the CAT spectrum and 17 minutes for the CORALIE spectrum.

For a previous application of mode identification in a pulsating star by means of cross-correlation functions we refer to Mathias & Aerts (1996). Another possibility to continue our monitoring is by means of FEROS. Up to now, we did not yet observe slowly pulsating B stars with this instrument, but we expect to find results comparable to those obtained with CORALIE.

3. Many Thanks

As already mentioned, a study as the one that we are undertaking is very challenging from an observational point of view. On the other hand, long-term monitoring is the only way to obtain meaningful results in the field of asteroseismology of early-type stars. Obviously, the OPC members judged that the scientific rationale of our proposals is important. We would like to thank both ESO and the Geneva Observatory for the generous awarding of telescope time to our long-term project.

We realise that the spectroscopic study of pulsating stars, one of the main subjects of our work in astronomy during the past 10 years, would not have been possible without an instrument like the CAT/CES. This combination of telescope and spectrograph was a cornerstone for the observational research performed at our institute, and several other astronomers, who now occupy key positions in important astronomical institutes, also made largely use of the CAT to develop their careers.

References

Aerts, C., 1994, Mode identification in pulsating stars, In IAU Symposium 162: Pulsation, Rotation and Mass Loss in Early-Type Stars, eds. L.A. Balona, H.F. Henrichs & J.M. LeContel, Kluwer Academic Publishers, 75.

Aerts, C., De Cat, P., Peeters, E., et al., 1999, Selection of a sample of bright southern Slowly Pulsating B stars for long-term photometric and spectroscopic monitoring, *A&A* **343**, 872.

Aerts, C., De Cat, P., Waelkens, 1998a, Slowly Pulsating B Stars – New Insights from Hipparcos, In *IAU S185*: New eyes to see inside the Sun and stars, eds. F. L. Deubner, J. Christensen-Dalsgaard, D. Kurtz, Kluwer Academic Publishers, 295.

Aerts, C., De Mey, K., De Cat, P., Waelkens, C., 1998b, Pulsations in early-type binaries, In *A Half Century of Stellar Pulsation Interpretations*, eds. P.A. Bradley & J.A. Guzik, A.S.P. Conference Series, Vol. **135**, 380.

Baade, D., 1998, Pulsations of OB-stars: new observations, In *IAU S185*: New eyes to see inside the Sun and stars, eds. F.L. Deubner, J. Christensen-Dalsgaard, D. Kurtz, Kluwer Academic Publishers, 347.

Dziembowski, W.A., Pamyatnykh, A.A., 1993, The opacity mechanism in B-type stars. I – Unstable modes in β Cephei star models, *MNRAS* **262**, 204.

Dziembowski, W.A., Jerzykiewicz, M., 1996, Asteroseismology of the β Cephei stars. I. 16 (EN) Lacertae, *A&A* **306**, 436.

Dziembowski, W.A., Jerzykiewicz, M., 1999, Asteroseismology of the β Cephei stars. II. 12 (DD) Lacertae, *A&A* **341**, 480.

Lomb, N.R., Shobbrook, R.R., 1975, New radial velocities and further photometric observations of λ Sco and κ Sco, *MNRAS* **173**, 709.

Mathias, P., Aerts, C., 1996, A spectroscopic analysis of the δ Scuti star 20 CVn, *A&A* **312**, 905.

Waelkens, C., 1987, Rotation and pulsation-mode-selection in B-type stars, In Stellar Pulsation, eds. A.N. Cox, W.M. Sparks, S.G. Starrfield, Springer-Verlag, 75.

Waelkens, C., Aerts, C., Kestens, E., et al., 1998, *A&A* **330**, 215.

Winget, D.E., Nather, R.E., Clemens, J.C., et al. ,1991, Asteroseismology of the DOV star PG1159–035 with the Whole Earth Telescope, *ApJ* **378**, 326.

A Procedure for Deriving Accurate Linear Polarimetric Measurements[1]

*H. LAMY and D. HUTSEMÉKERS**

Institut d'Astrophysique, Université de Liège, Belgium; e-mail: lamy@astro.ulg.ac.be, hutsemek@astro.ulg.ac.be

We present here a procedure written within the ESO MIDAS reduction package with the aim of deriving semi-automatically linear polarisation data from CCD images obtained with beam-splitters such as those available at the ESO 3.6-m telescope equipped with EFOSC2 or at the VLT equipped with FORS1. This method is adequate for point-like objects and was used for measuring quasar polarisation (cf. Hutsemékers et al. 1998). We also report on the detection of a significant image deformation effect, most probably due to the recent addition to EFOSC2 of a rotatable half-wave plate.

Polarimetry with EFOSC2

With EFOSC2, polarimetry is performed by inserting in the parallel beam a Wollaston prism which splits the incoming light rays into two orthogonally po-larised beams separated by a small angle (typically 20″). Every object in the field has therefore two images on the CCD detector (see Figure 1). In order to avoid any overlapping of different images and to reduce the sky contribution, an aperture mask is put at the focal plane of the telescope. The normalised Stokes parameters (NSPs), q and u, fully describing the linear polarisation, are then computed from the fluxes measured in the two orthogonally polarised images. Two frames with the Wollaston prism rotated by 45° are necessary to determine the NSPs. Additional frames may be considered although the quasi-perfect transmission of the Wollaston generally makes two orientations sufficient (Serkowski 1974; di Serego Alighieri 1989). Usually the orientations at 270° and 225° are taken and

$$q = \frac{I^{\mathrm{u}}_{270} - I^{\mathrm{l}}_{270}}{I^{\mathrm{u}}_{270} + I^{\mathrm{l}}_{270}}, \quad u = \frac{I^{\mathrm{u}}_{225} - I^{\mathrm{l}}_{225}}{I^{\mathrm{u}}_{225} + I^{\mathrm{l}}_{225}}, \qquad (1)$$

---

[1] See note on page 31.

*Chercheur Qualifié au Fonds National de la Recherche Scientifique (Belgium).

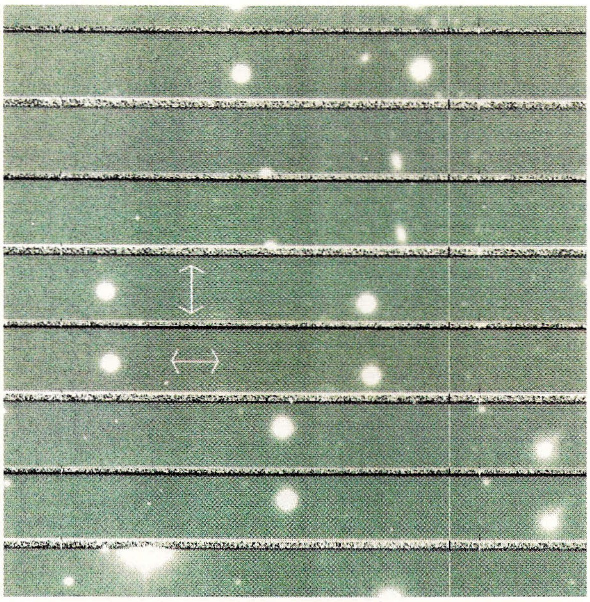

Figure 1: Example of a CCD frame obtained with EFOSC2, a Wollaston prism in the grism wheel and a mask at the focal plane of the telescope. Every object in the field has two orthogonally polarised images separated by ~ 20″ and called upper and lower images in the text. The arrows illustrate the direction of the polarisation of the two images. The y-axis is defined along the columns of the CCD, which is roughly the direction of the splitting. The detector was the Loral/Lesser CCD #40 with a pixel size of 0.160″ on the sky. The target was the quasar M08.02, observed on April 27, 1998 in the V filter with an exposure time of 300 s. It has a degree of polarisation $p \simeq 1.4\%$.

where I^{u}_{α} and I^{l}_{α} respectively represent the integrated fluxes from the upper and the lower images of the object produced by the Wollaston prism set at a position angle α. The associated errors, σ_q and σ_u, are calculated by computing the errors from the read-out noise and the photon noise in the object and the sky background and then by propagating these errors in Eq.1. The degree of polarisation is given by $p = \sqrt{q^2+u^2}$ and the polarisation position angle by $\theta = 1/2 * \arctan(u/q)$. The angles are measured relative to the instrument reference frame such that the observation of at least one polarimetric standard star is required for determining the polarisation position angle zero point.

Within this observing mode, the whole instrument has to be rotated, which means significant time-loss mainly due to re-pointing the objects. The insertion of a rotating half-wave plate (HWP) as the first optical element in the parallel beam significantly fastens the procedure by keeping EFOSC fixed (Schwartz & Guisard, 1995). Usually, four frames with the HWP orientated at 0°, 22.5°, 45° and 67.5° are taken and the NSPs are derived using the following formulae (e.g. di Serego Alighieri 1998):

$$q = \frac{R_q - 1}{R_q + 1} \text{ where } R_q = \frac{I^{\mathrm{u}}_{0}/I^{\mathrm{l}}_{0}}{I^{\mathrm{u}}_{45}/I^{\mathrm{l}}_{45}}, \tag{2}$$

$$u = \frac{R_u - 1}{R_u + 1} \text{ where } R_u = \frac{I^{\mathrm{u}}_{22.5}/I^{\mathrm{l}}_{22.5}}{I^{\mathrm{u}}_{67.5}/I^{\mathrm{l}}_{67.5}},$$

I^{u}_{β} and I^{l}_{β} respectively denoting the integrated fluxes from the upper and the lower images of the object produced by the Wollaston prism. β is the position angle of the HWP. The polarisation degree, the polarisation position angle and the associated errors are calculated as above. In principle each NSP may also be evaluated from a single frame using Eq. 1 such that, if we call q_0 (resp. q_{45}) the NSP calculated from the fluxes measured on the frame obtained with the HWP set at position angle 0° (resp. 45°), we should have $q_0 \simeq -q_{45}$.

Since the polarisation observed in extragalactic objects is usually ~ 1%, a careful subtraction of the sky background and an accurate determination of the object intensities I^{u} and I^{l} are essential to achieve a good estimate of the NSPs. In the next section we describe a MIDAS procedure written with the aim of optimising these two constraints.

The Reduction Procedure

In order to accurately measure I^{u} and I^{l}, the first step is to subtract locally the sky background. Since the latter is usually polarised, this must be done independently for each orthogonally polarised image. For that purpose, two strips centered on the object are first extracted. Then the local sky is evaluated by fitting a bi-dimensional polynome to values of the background measured in small boxboxes free of cosmic rays and faint objects. The best results were obtained with polynomes of degree one. The small boxes are chosen in the upper and in the lower strips at exactly the same locations with respect to the object, taking into account a possible misalignment between the direction of the image splitting and the columns of the CCD.

Secondly, we noted after several trials that the usual standard aperture photometric methods available in MIDAS are not accurate enough for polarimetry: these procedures generally measure the total flux inside a given circle, taking entirely into account those pixels which are only partially contained in the circle. This is particularly problematic when the pixel size is large. Instead, we determine the center and the width of the object image at subpixel precision by fitting a bi-dimensional gaussian profile. Then, by means of a FORTRAN code, we integrate the flux in a circle of same center and arbitrary radius, taking into account only those fractions of pixels inside the circle. This was achieved on the basis of simple geometrical considerations. The NSPs may then be evaluated for any reasonable value of the aperture radius, expressed in units of the mean gaussian width $\sigma = (2\ln2)^{-1/2}$FWHM/2, which is assumed to be identical for both the upper and lower images of the object. In order to take as much flux as possible without too much sky background, we adopt the radius $R/\sigma = 2.5$ which generally fulfils these requirements. Typical results obtained with the Wollaston prism only (i.e. without a HWP) indicate that, within the error bars, the measured NSPs are very stable against aperture radius variation, therefore giving confidence in the method.

With the aim of providing a semi-automatic and easy-to-use tool for extracting polarimetric data, two procedures have been implemented in MIDAS. The first one measures the intensities of the object and that of the background for any desired value of the aperture radius.

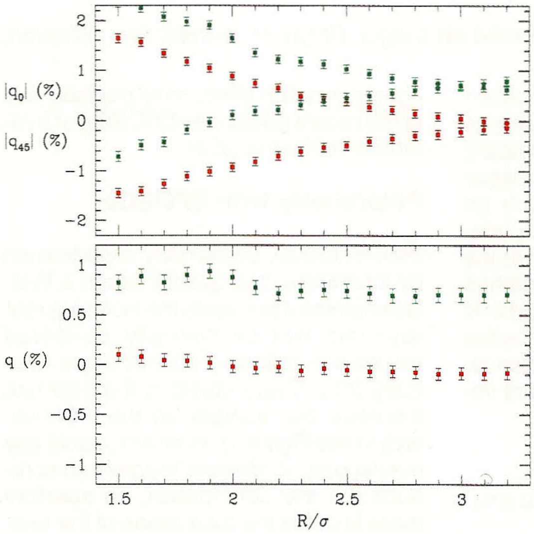

Figure 2: Upper panel: The normalised Stokes parameters, q_0 and q_{45}, are represented in absolute values as a function of the aperture radius expressed in units of the gaussian width of the image, for a polarised and an unpolarised quasar. These data were obtained on April 27–28, 1998 with EFOSC2 equipped with a 20″ Wollaston prism and a Half-Wave Plate set at 0° and 45°. The quasars were observed in the V filter with a typical exposure time of 300s for a given orientation. The pixel size was 0.130″ on the sky. Lower panel: The normalised Stokes parameter, q, computed according to Eq. 2 (see text). q is essentially stable against radius variation indicating that the effect described in the text is corrected.

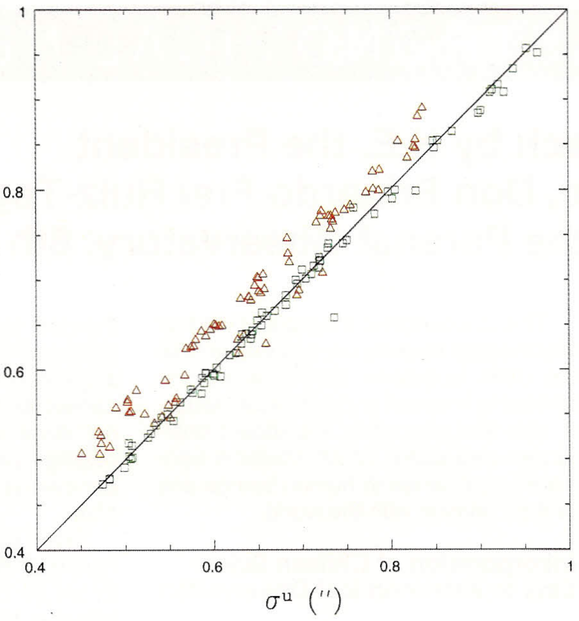

Figure 3: The gaussian widths of the lower images, σ^l, are represented as a function of the widths of the upper ones, σ^u, for all quasars observed during the nights 27–28 April 1998. Note that four HWP orientations have been obtained for each object and are presented here. The green squares represent σ_x and the red triangles σ_y. Most of the objects show an elongation along the direction of the Wollaston splitting (y-axis). The gaussian widths are expressed in arcsecond. The lack of corresponding red triangles in the right top corner corresponds to the second image deformation described in the text, affecting objects with wider profiles only.

The second one combines these measurements to provide the NSPs, the errors, the degree of polarisation and the polarisation position angle as a function of the aperture radius. The procedures can be made available as such to anyone interested.

Image Deformations and Their Effect on the Measurements

While the dependence of the NSPs against radius variation is quite flat when using the Wollaston without HWP, a different behaviour is found when adding the HWP. As previously stated, q_0 and q_{45} should be identical in absolute value apart from a small difference due to instrumental polarisation. However, it appears that $|q_0|$ and $|q_{45}|$ measured for a given aperture radius significantly differ. This is illustrated in the upper panel of Figure 2: for small radii, $|q_0|$ and $|q_{45}|$ appear quite different (sometimes ≥ 1%), while they finally tend towards the same value as the radius increases. For $R/\sigma \geq 3$, they are equal within the error bars. The two curves have nearly symmetrical shapes with respect to the expected behaviour (i.e. a flat curve with $|q_0|$ and $|q_{45}|$ identical). This effect is detected for polarised and unpolarised objects.

By fitting a bi-dimensional gaussian profile to the object, we have measured the widths σ_x and σ_y of the upper and lower orthogonally polarised images of the object. Figure 3 represents σ_x^l (resp σ_y^l), measured from the lower image, as a function of σ_x^u (resp σ_y^u), measured from the upper image, for every CCD frame obtained during the nights April 27–29, 1998. It appears clearly that the lower images are systematically more elongated along the y-axis than the upper images, while their widths are nearly identical along the x-axis direction. The mean difference between σ_y^l and σ_y^u is ~ 0.08″. This difference is more or less constant whatever the mean width of the gaussian profile. It is also independent of the HWP position angle. As a consequence, for a given aperture radius, we measure less flux in the upper images than in the lower ones. Therefore, for small radii, $|q_0|$ appear larger and $|q_{45}|$ smaller than the actual values. As the aperture radius increases, the total flux of the lower image is progressively taken into account and this effect vanishes, $|q_0|$ and $|q_{45}|$ tending towards the same value, in agreement with the behaviour seen in Figure 2. Note that there are a few frames on which the object images have $\sigma_y^u \sim \sigma_y^l$ which precisely corresponds to those cases where the $|q_0|$and $|q_{45}|$ curves are more similar.

Fortunately, due to the fact that the image deformations are independent of the HWP orientation, this effect is well corrected when determining a given NSP by combining the intensities from two frames according to Eq. 2. This is illustrated in the lower panel of Figure 2 which shows the expected flat curves. We may therefore conclude that two frames with the HWP set at angles separated by 45° are necessary to accurately evaluate one of the NSPs. If only a single frame is obtained, the NSP has to be measured with a radius large enough to minimise the effect. In this latter case, the radius $R/\sigma = 3$ is generally sufficient and the additional noise due to the background not too large. Note that, in fact, none of the two orthogonally polarised images is actually circular, as illustrated in Figure 4. But only the image deformations differentially affecting the upper and lower images have an effect on the NSPs measurements. It is important to emphasise that these effects were not visible on frames obtained previously with the Wollaston prism only, suggesting that the HWP is most probably responsible for the observed image deformations.

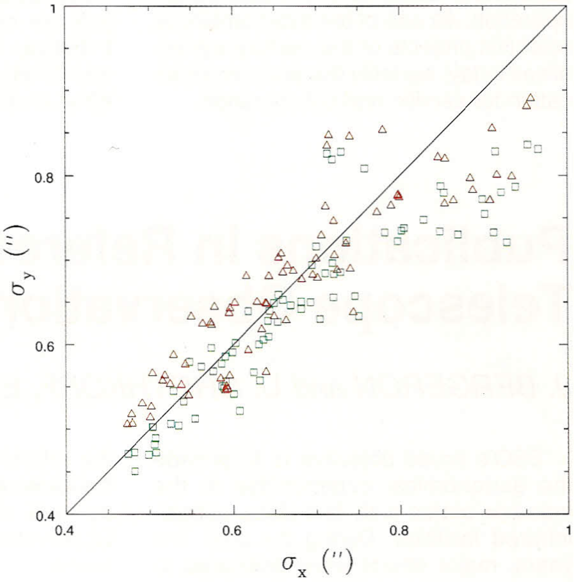

Figure 4: The gaussian width σ_y is represented as a function of σ_x for the upper (green squares) and the lower (red triangles) object images considering the same data as in Figure 3. The gaussian widths are expressed in arcseconds. The general trend is that upper images have $\sigma_x^u > \sigma_y^u$ while the lower images have $\sigma_x^l < \sigma_y^l$. For images with larger profiles, both images flatten ($\sigma_x > \sigma_y$), the difference being roughly constant.

The image deformations described here appear much more complex than the expected behaviour due to the Wollaston chromatism only (e.g. di Serego Alighieri et al. 1989). Such an effect is important to further investigate and understand since it may affect imaging polarimetry with high spatial resolution instruments as will be available on the VLT.

Acknowledgements

This research is supported in part by contract ARC94/99-178 and by contract PAI P4/05. We also thank Marc Remy for providing us with the FORTRAN code.

References

di Serego Alighieri S. 1989, In:Grosbøl P.J. et al (eds.) 1st ESO/ST-ECF, Data Analysis Workshop, 157.

di Serego Alighieri S. 1998, in *Instrumentation for Large Telescopes*, Ed. J.M. Rodriguez Espinosa, Cambridge University Press, 287.

Hutsemékers D., Lamy H. & Remy M. 1998, *A&A* **340**, 371.

Schwarz H., Guisard D. 1995, *The Messenger* **81**, 9.

Serkowski K., 1974, in Methods of Experimental Physics, vol. 12, part A, eds. M.L. Meeks & N.P. Carleton (New York: Academic Press), 361

Erratum

In the June issue of *The Messenger* (No. 96), page 26 (article by H. Lamy and D. Hutsemékers), formula 2 should read:

$$\begin{aligned} q &= \frac{R_q - 1}{R_q + 1} \text{ where } R_q^2 = \frac{I_0^{\mathrm{u}}/I_0^{\mathrm{l}}}{I_{45}^{\mathrm{u}}/I_{45}^{\mathrm{l}}}, \\ & \qquad\qquad\qquad\qquad\qquad\qquad\qquad (2) \\ u &= \frac{R_u - 1}{R_u + 1} \text{ where } R_u^2 = \frac{I_{22.5}^{\mathrm{u}}/I_{22.5}^{\mathrm{l}}}{I_{67.5}^{\mathrm{u}}/I_{67.5}^{\mathrm{l}}}, \end{aligned}$$